Biophysical Journal Volume 84 May 2003 3007–3021

Distinctive Modulatory Effects of Five Human Auxiliary β_2 Subunit Splice Variants on L-Type Calcium Channel Gating

Shoji X. Takahashi,* Scott Mittman,† and Henry M. Colecraft*

Calcium Signals Laboratory, *Department of Biomedical Engineering, †Department of Anesthesiology, Johns Hopkins University School of Medicine, Baltimore, Maryland

ABSTRACT Sequence analysis of the human genome permitted cloning of five Ca^{2+}-channel β_2 splice variants (β_{2a}–β_{2e}) that differed only in their proximal amino-termini. The functional consequences of such β_2-subunit diversity were explored in recombinant L-type channels reconstituted in HEK 293 cells. β_{2a} and β_{2e} targeted autonomously to the plasma membrane, whereas β_{2b}–β_{2d} localized to the cytosol when expressed in HEK 293 cells. The pattern of modulation of L-type channel voltage-dependent inactivation gating correlated with the subcellular localization of the component β_2 variant—membrane-bound β_{2a} and β_{2e} subunits conferred slow(er) channel inactivation kinetics and displayed a smaller fraction of channels recovering from inactivation with fast kinetics, compared to β_{2b}–β_{2d} channels. The varying effects of β_2 subunits on inactivation gating were accounted for by a quantitative model in which L-type channels reversibly distributed between fast and slow forms of voltage-dependent inactivation—membrane-bound β_2 subunits substantially decreased the steady-state fraction of fast inactivating channels. Finally, the β_2 variants also had distinctive effects on L-type channel steady-state activation gating, as revealed by differences in the waveforms of tail-activation (*G-V*) curves, and conferred differing degrees of prepulse facilitation to the channel. Our results predict important physiological consequences arising from subtle changes in Ca^{2+}-channel β_2-subunit structure due to alternative splicing and emphasize the utility of splice variants in probing structure-function mechanisms.

INTRODUCTION

High-voltage-activated (HVA) Ca^{2+} channels transduce electrical signals into diverse and essential processes such as muscle contraction, synaptic transmission, and gene expression. HVA Ca^{2+} channels are hetero-multimers comprised minimally of pore-forming α_1, and auxiliary β and $\alpha_2\delta$ subunits. The rich variety of physiological responses mediated by HVA Ca^{2+} channels is mirrored by an equally impressive molecular diversity of individual subunits—seven genes encoding α_1 subunits (α_{1A}–α_{1F}, α_{1S}), four encoding β subunits (β_1–β_4), and three encoding $\alpha_2\delta$ subunits ($\alpha_2\delta$-1 to $\alpha_2\delta$-3), have been identified (for review, see Catterall, 2000).

Auxiliary β subunits are potent determinants of Ca^{2+} channel behavior. Qualitatively, all four β-subunit isoforms act similarly to markedly increase surface membrane expression of co-expressed α_1-subunits (Chien et al., 1995; Brice et al., 1997; Gao et al., 1999; Yamaguchi et al., 2000), dramatically enhance Ca^{2+} current amplitude over that obtained with α_1 alone (Singer et al., 1991; Jones et al., 1998), and produce hyperpolarizing shifts in the voltage-dependence of channel activation (Singer et al., 1991; Perez-Reyes et al., 1992; De Waard et al., 1994). Just as important, there are significant distinctions in the properties of the different β-subunit isoforms with respect to their tissue distribution (Castellano et al., 1993a,b; Ludwig et al., 1997; Pichler et al., 1997), subcellular localization (Colecraft et al., 2002), and impact on channel inactivation kinetics (Olcese et al., 1994; De Waard and Campbell, 1995; Wei et al., 2000; Colecraft et al., 2002). Such functional diversity of Ca^{2+} channel β subunits is a likely contributor to the broad repertoire of physiological responses supported by HVA Ca^{2+} channels.

Alternative splicing generates an even greater molecular diversity of β subunits, potentially extending the physiological dimensions of HVA Ca^{2+} channel functions (Collin et al., 1993; Cahill et al., 2000; Helton and Horne, 2002). Presently, however, knowledge of the full complement of β-subunit splice variants that are expressed, and the biophysical and physiological traits that they impart, remains relatively obscure. Two key reasons for this impasse can be identified. First, discovery of β-subunit variants has been driven primarily by traditional cloning methods that usually identify only one or a few members of a splice variant population at a time (Hullin et al., 1992; Perez-Reyes et al., 1992; Castellano et al., 1993a,b; Helton and Horne, 2002). Second, even when splice variants of a given β subunit are known, the biophysical properties conferred by the distinct β-splice forms to a given channel are rarely rigorously compared.

Research relating to splice variation in the Ca^{2+} channel β_2 subunit epitomizes these deficiencies. β_2 is the dominant β subunit expressed in heart (Perez-Reyes et al., 1992; Pichler et al., 1997; Haase et al., 2000) and retina (Ball et al., 2002), but is also an important component of HVA Ca^{2+} channels expressed in brain (Ludwig et al., 1997; Pichler et al., 1997), smooth muscle (Reimer et al., 2000), and

Submitted September 12, 2002, and accepted for publication January 28, 2003.

Address reprint requests to Henry M. Colecraft, Calcium Signals Laboratory, Dept. of Biomedical Engineering, Johns Hopkins University School of Medicine, 720 Rutland Ave., 726 Traylor Bldg., Baltimore, MD 21205. Tel.: 410-955-0072; Fax: 410-614-8269; E-mail: hcolecra@bme.jhu.edu.

0006-3495/03/05/3007/15 $2.00

pancreas (Iwashima et al., 2001). Five distinct β_2 subunits, varying only in the proximal amino terminus, have been cloned from different species including rat (Perez-Reyes et al., 1992), rabbit (Hullin et al., 1992), human (Rosenfeld et al., 1993), and mouse (Massa et al., 1995). To date, however, no more than three of the β_2 forms have been identified in any one species (Qin et al., 1998), rendering it ambiguous whether they represent bona fide splice variants of the β_2 gene. Also, aside from the first β_2 subunit cloned, β_{2a}, the biophysical properties of the different β_2 variants have not been rigorously explored. This constitutes a critical impediment to understanding the physiological implications of having distinct β_2 variants expressed in different tissues.

The recently published draft of the human genome sequence provides new opportunities to identify and clone novel splice variants of a given gene. Here, guided by genomic sequence analysis, we cloned all five β_2 splice variants from human heart and brain cDNA libraries. The biophysical properties of the different β_2 variants were explicitly compared in recombinant L-type (Ca_V 1.2; Ertel et al., 2000) Ca^{2+} channels (α_{1C}, β_2, $\alpha_2\delta$) reconstituted in HEK 293 cells. We found fundamental qualitative and quantitative distinctions among the subtly divergent β_2-splice variants with respect to their subcellular localization and influence on L-type channel gating, providing new insights into structure-function mechanisms underlying α_{1C}–β_2-subunit interactions.

METHODS

Molecular cloning

To identify novel human Ca^{2+} channel β_2 splice variants, we searched the HTGS database using TBLASTN algorithm with peptide query sequences derived from human (β_{2a} and β_{2d}) or other vertebrate species (β_{2b}, β_{2c}, and β_{2e}). In some cases, either because of short peptide length or sequence differences, the TBLASTN search was not sensitive enough to find orthologous human sequences. In those cases, more sensitive similarity searches were performed on the draft BAC sequences identified in the first round of searches to locate the remaining sequences. The complete open reading frames of the five Ca^{2+} channel β_2 splice variants were amplified from human brain (β_{2a}, β_{2c}, β_{2d}, and β_{2e}) and heart (β_{2b}) cDNA libraries (Clontech) by PCR. Upstream primers for the PCR reactions were designed using sequence information from public databases. β_{2a}, β_{2b}, and β_{2e} were amplified with the respective sense primers TCTGCCCCGCTAGCATGCAGTGCTGCGGGCTGGT, GGAATTGGGCTAGCATGCTTGACAGACGCCTTAT, GCGCTGTCGCTAGCATGAAGGCCACCTGGAT, and the antisense primer ACAAAAGGGCAGAATTCATTGGGGGATGTAAACA. Reactions contained 1 μl cDNA, 400 nM each primer, 200 μM each dNTP, 1.8 mM Mg^{2+} and 1 unit ELONGASE enzyme mix with its recommended buffer system in a total volume of 25 μl. Amplification was with a touchdown protocol with tubes held at 94°C for 30 s, a variable annealing temperature for 30 s, and extension at 68°C for 120 s. The initial cycle annealing temperature was 64°C; in each of the subsequent five cycles the annealing temperature was 0.5°C lower. In all subsequent cycles, the annealing temperature was 61°C. β_{2a} and β_{2b} PCR products were TA cloned into pCR2.1, and then cloned by *Nhe*I and *Eco*RI sites into the bicistronic expression vector pAd IR (Alseikhan et al., 2002), which contains a CMV promoter followed sequentially by a multiple cloning site, an internal ribosomal entry site sequence, and GFP cDNA. In this configuration, upon transfection into mammalian cells, β_2-subunits and GFP are translated as independent protein entities from the same mRNA transcript. This permits GFP fluorescence to be directly used to verify cell transfection.

For β_{2c} and β_{2d}, a first round of amplification was performed with the following sense primers AGGGGAGTGGACTGGACCTG and AAAGGGACATGTCCAAGTCGCCTCCCACAG, and antisense primer GTTTTGGGGATGCTGTTAGT. Touchdown during the first 20 cycles was followed by 12 cycles with annealing temperature of 54°C. These amplicons were then gel-purified and reamplified with the respective sense primers CACATGGGCTAGCATGAATCAGGGGAGTGGACTGGACCTG and CCGACTTTGCTAGCATGGTCCAAAGGGACATGTCCAAGT, and antisense primer ACAAAAGGGCAGAATTCATTGGGGGATGTAAACA. Due to the relatively high rate of misincorporation with PCR amplification, most clones contained errors. Therefore, once one error-free clone of the β_{2b}-splice variant (in pAd IR) had been identified, it served as the backbone for substitution of error-free versions of the four other D1 sequences via *Nhe*I and *Hin*dIII restriction sites. For GFP fusion constructs of β_2 subunits, their complete coding sequences up to the penultimate codon were PCR amplified with high fidelity *Pfu* polymerase using as template the β_2 subunits in pAd IR described above. Sense primers (as above) were used in conjunction with the antisense primer AGGATCCTTGGGGGATGTAAACATCCCTG. The PCR products were sequenced and cloned into the expression vector pAdCMV EGFP-N3 (Colecraft et al., 2002) using *Nhe*I and *BamH*I sites, yielding pAd CMV β_{2a-e}-GFP. The cloned β_2 variant sequences have been deposited in GenBank with the following accession numbers: β_{2a} AF423189, β_{2b} AF285239, β_{2c} AF423190, β_{2d} AF423191, and β_{2e} AF423192.

Transfection of HEK 293 cells

Low-passage number HEK 293 cells were maintained as previously described (Brody et al., 1997). The calcium-phosphate precipitation method was used to transfect 10 μg each of cDNA encoding wild-type rabbit α_{1C} (Wei et al., 1991), rat $\alpha_2\delta$ (Tomlinson et al., 1993), and the appropriate β_2 splice variant (subunits).

Confocal imaging

β_2-GFP fusion constructs were transiently transfected into HEK 293 cells, and confocal images were acquired 48 h posttransfection using a Zeiss laser-scanning confocal microscope. Exemplar intensity images were low-pass filtered and analyzed offline using custom-written software in MATLAB 6.0, Release 12 (Mathworks, Natick, MA).

Electrophysiology

Whole-cell recordings were obtained at room temperature 2–3 days after transfection using an Axopatch 200A patch-clamp amplifier (Axon Instruments, Union City, CA). Cells were continuously perfused with external solution containing (in mM): 140 TEA-$MeSO_3$, 10 HEPES, and 5 $BaCl_2$ (pH 7.3, adjusted with TEA-OH). The internal solution contained (in mM): 135 Cs-$MeSO_3$; 5 $CsCl_2$; 0.5 EGTA; 1 $MgCl_2$; 4 MgATP; and 10 HEPES (pH 7.3, adjusted with CsOH). Solution osmolarities were adjusted to 290–300 mOsm with glucose. Series resistances were typically 1–2 MΩ after >70% compensation.

Currents were sampled at 10 kHz and filtered at 2 kHz, except for tail-activation protocols, in which currents were sampled at 25 kHz and filtered at 10 kHz. Voltage protocols were delivered at 60-s intervals, and leak and capacitive transients were subtracted by P/8 protocol.

Data and statistical analysis

Data were analyzed using custom-written software in MATLAB and Microsoft Excel, and are displayed as mean values ± SE. Recovery from inactivation, steady-state inactivation, and steady-state activation were well-

TABLE 1 Comparison of Boltzmann parameters among β_2 splice variants

	h(20 s) $V_{1/2}$ (mV)	Recovery F_{fast}	Activation F_{low}
β_{2a}	−41	0.51	0.70
β_{2b}	−45	0.73	0.36
β_{2c}	−41	0.66	0.51
β_{2d}	−41	0.72	0.61
β_{2e}	−38	0.52	0.99

Values were determined using least-squares criteria. For steady-state inactivation, $k = 8.6$ mV. For recovery from inactivation, $\tau_1 = 91.6$ ms and $\tau_2 = 20$ s. For activation, $V_{½,low} = -2$ mV, $V_{½,high} = 38$ mV, $k_{low} = 10$ mV, and $k_{high} = 20$ mV.

TABLE 2 Parameters for quantitative kinetic model of β_2 splice variants

	Activation constants				Allosteric factors		Inactivation constants	
	$\alpha(V)$	$\beta(V)$	γ	δ	f	h	k_i	k_r
Fast (ms^{-1})	1.0	0.8	1.5	1.0	0.25	0.25	3.E-03	1.E-03
Slow (ms^{-1})	1.0	0.8	1.5	1.0	0.25	0.25	4.E-04	4.E-06

Rate constants correspond to transitions diagrammed in Fig. 8 *A*, Scheme 1. $\alpha(V)$ and $\beta(V)$ are voltage-dependent rate constants using Hodgkin-Huxley formalism. In simulations, relative contributions of fast to slow channels were given by F_{fast} values determined from the recovery from inactivation protocol.

described by the following equations, with parameters (Table 1) determined using least-squares criteria.

Recovery from inactivation data were fitted by a biexponential function of the form: $RF = 1 - [F_{fast} \times \exp(-t/\tau_1) + (1 - F_{fast}) \times \exp(-t/\tau_2)]$, where F_{fast} is the fraction of the fast-recovery component, t is the interpulse duration, and τ_1 and τ_2 are the fast- and slow-recovery time constants, respectively.

Steady-state inactivation data were fitted by a Boltzmann function of the form: $h(20\text{ s}) = I_2/I_1 = 1/(1 + \exp((V - V_{½})/k))$, where I_2 is the test-pulse current, I_1 is the normalization current, V is the membrane potential of the conditioning pulse, $V_{½}$ is the potential for half-inactivation, and k is the slope factor.

Steady-state activation data were fitted by a dual-Boltzmann function of the form: $G/G_{max} = F_{low}/(1 + \exp(V_{½,low} - V)/k_{low}) + (1 - F_{low})/(1 + \exp(V_{½,high} - V)/k_{high}))$, where G is the tail current, G_{max} is the tail current evoked by a depolarization to +110 mV, F_{low} is the fraction of the low-threshold component, V is the membrane potential of the test pulse, $V_{½,low}$ and $V_{½,high}$, and k_{low} and k_{high} are the half-activation potentials and slope factors for the low- and high-threshold components, respectively.

Kinetic modeling

Stochastic simulations were performed in MATLAB using the built-in matrix exponential function (*expm*) to solve an 11-state Markov chain for transition probabilities (Colquhoun and Hawkes, 1981). Repeated matrix exponential calls were made with a step size of 400 μs, and ionic currents were calculated assuming a linear conductance for Ba^{2+} with a reversal potential of +132 mV. Voltage-dependent transitions were modeled with rate constants of the form: $k_{ij}(V) = k_{ij} \times \exp(z_{ij} \times V \times F / RT)$, where k_{ij} is a rate constant (in ms^{-1}) at zero membrane potential associated with the i-to-j transition, z_{ij} is the valence of the gating charge (set to one elementary charge for simplicity), V is the membrane potential (in mV), and RT/F is the gas constant and absolute temperature divided by Faraday's constant (equal to +25 mV). The final transition between closed and open states within each mode was modeled as voltage-independent (Zagotta and Aldrich, 1990; Colecraft et al., 2002) and set to the approximately ms timescale of rapid openings and closings during L-type Ca^{2+} channel bursts (Colecraft et al., 2002). The maximum P_o was set to 0.6. Parameters were optimized by eye. Fig. 8 *C*, Scheme 2, and Table 2 provide kinetic structure and detailed rate constants used in the simulations.

RESULTS

Genomic perspective permits in silico cloning of novel human β_2-splice variants

Primary sequence homology between β subunits suggests a modular domain structure (domains D1–D5; Fig. 1 *A*) in which three variable regions (D1, D3, and D5) are interspersed by two conserved domains (D2 and D4; see De Waard et al., 1994; Birnbaumer et al., 1998). A search of public databases revealed the existence of five β_2-subunit forms, varying only in the D1 domain, distributed among different species (Colecraft et al., 2002). Presently, no more than three of the β_2 forms have been cloned from any one species, making it uncertain whether they constitute genuine splice variants, or simply reflect species variation. The availability of human genomic sequence in the form of draft BAC sequences originally provided a unique opportunity to resolve this core ambiguity. A search of the HTGS database using TBLASTN (as described in Methods) yielded positive outcomes that explicitly confirmed the presence of sequences for all five D1 domains within the human β_2 gene. Therefore, we have designated them β_{2a}–β_{2e}, with the alphabetical order corresponding to their chronological identification in the different species and not their order in the genome (Fig. 1 *B*; see also Colecraft et al., 2002). This nomenclature supplants previous assignments that were primarily species-based and suffered from lack of a clear recognition that there exist at least five distinct D1 domain splice variants of β_2.

The existence of a contiguous genomic DNA sequence, in which all five D1 variants could be identified, fully illuminated the relative orientation of the corresponding exons in the β_2 gene (Fig. 1, *B* and *C*). As shown in Fig. 1 *C*, the five D1 variants result from the alternative splicing of six exons. Exon 7, a constitutive exon that encodes the beginning of the D2 domain common to all β_2 variants, is the acceptor exon in four mutually exclusive splicing pathways. β_{2a} arises from splicing between donor exon 5 and acceptor exon 7. For variants β_{2b} and β_{2e}, exons 4 and 6 serve as donor exons, respectively. β_{2c} and β_{2d} share a common 31-amino-acid sequence just upstream of domain D2; for these variants, splicing occurs between exons 3 and 7. Exon 3 lacks an initiation codon. Splicing occurs between either of donor exons 1 or 2 and acceptor exon 3 to give rise to the β_{2d} and β_{2c} transcripts, respectively. Although not addressed in this study, β_2 transcripts also exhibit variability in domain D3, arising from mutually exclusive splicing of exons 11 (134 nt), 12 (20 nt), and 13 (62 nt) (Colecraft et al., 2002).

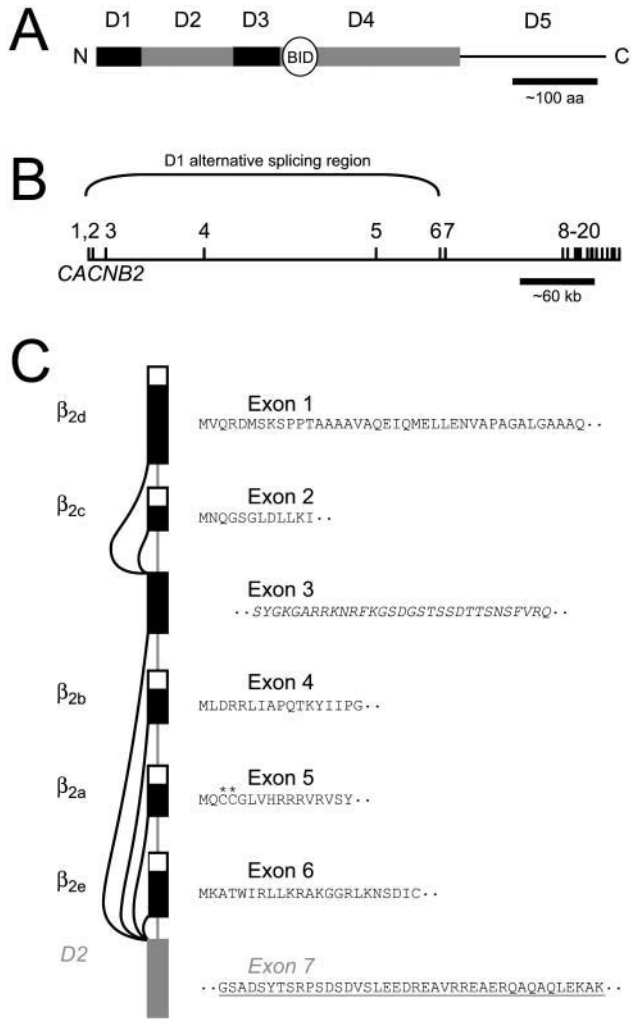

FIGURE 1 Genomic perspective clarifies basis of Ca^{2+} channel β_2-subunit molecular diversity. (*A*) Modular domain structure proposed for Ca^{2+}-channel β subunits based on primary sequence identity. Two conserved domains (D2 and D4, *gray boxes*) are interspersed by three variable domains (D1, D3, and D5). D1 is an important determinant of channel inactivation, and D4 contains the β-interaction domain, important for interactions with pore-forming α_1-subunits. Alternative splicing of β_2 is known to occur in at least two regions, D1 and D3 (*black boxes*). (*B*) Schematic structure of human *CACNB2* based on analysis of human genomic DNA sequence. Exons are represented by vertical lines and introns by horizontal lines; introns are approximately to scale, whereas exons are not to scale. (*C*) Schematic of mutually exclusive splicing patterns of exons 1–6 that result in the generation of five alternative β_2-subunit D1 domains. The corresponding amino acid sequences are represented. Exons 1, 2, and 4–6 encode the amino-termini of the distinct β_2 splice variants; each has their own initiation codon and 5′ untranslated region (*white box*). Exon 3 is common to β_{2c} and β_{2d}. Exon 7 (*gray box*, with underlined sequence) is a constitutive exon that encodes the beginning of the D2 domain common to all β_2 variants.

β_{2a}–β_{2e} transcripts described herein all contain exon 11 and lack exons 12 and 13.

Despite the predicted existence of at least five human β_2 D1 splice variants, only β_{2a} and β_{2d} have thus far been cloned from human tissue (Rosenfeld et al., 1993; Yamaguchi et al., 2000). Armed with sequence information from the human genome, we designed primers that permitted the successful amplification of the open reading frames of all five variants from human heart (β_{2b}) and brain (β_{2a}, β_{2c}–β_{2e}) cDNA libraries. Having thus established the presence of β_{2a}–β_{2e} transcripts in human tissues, we next sought to determine the functional consequences of such β_2-subunit diversity.

Distinctive subcellular targeting of β_2-splice variants

The bulk of published work on Ca^{2+} channel β_2-subunits has centered on β_{2a}, the earliest cloned splice variant. A key distinguishing trait of β_{2a} is that, when expressed alone in heterologous systems, it targets to the plasma membrane —an observation at odds with predictions that it would localize to the cytosol (Chien et al., 1995). This anomalous behavior is due to palmitoylation of two cysteines residing in the D1 domain (Chien et al., 1996; see also Fig. 1 *C*) and is the underlying basis for several unique functional hallmarks of β_{2a}. None of the other β_2-splice variants (β_{2b}–β_{2e}) retain consensus sequences for palmitoylation (Milligan et al., 1995; Resh, 1999), raising expectations that they would differ from β_{2a} with respect to membrane targeting and any attendant functional sequelae. Nevertheless, since it is difficult to predict with certainty the subcellular localization of a protein, and because this feature is a vital prognosticator of β-subunit function (Qin et al., 1998), we first sought to compare the subcellular targeting of heterologously expressed β_2 variants.

To directly visualize β_2-subunit localization in living cells, we expressed GFP-fusion constructs of β_{2a}–β_{2e} in HEK 293 cells and viewed cellular GFP fluorescence by confocal microscopy (Fig. 2). Cells expressing GFP alone displayed bright green fluorescence throughout the cell, with equal intensity in the nuclear and cytoplasmic compartments (not shown). Reassuringly, β_{2a}-GFP localized to the periphery of the cell, a clear indication that fusion of GFP to the carboxyl terminus did not disrupt the well-known membrane targeting of β_{2a}. In accord with their lack of consensus sites for palmitoylation and relatively high molecular weights (>90 kDa), β_{2b}–β_{2d} were localized to the cytosol and excluded from the nucleus (molecular weight cutoff for passive diffusion into the nucleus is 40 kDa; Davis, 1995). By contrast, β_{2e}-GFP displayed plasma membrane targeting, akin to that observed with β_{2a} (Fig. 2). This novel observation was completely unexpected given the hydrophilic character of the β_{2e} D1 domain and serves to underscore uncertainties associated with a priori prediction of β-subunit subcellular location.

These results firmly established that β_2-splice variants divided into two camps with respect to subcellular localization—β_{2a} and β_{2e} target to the plasma membrane, while β_{2b}–β_{2d} are present in the cytosol. Co-expression of GFP-

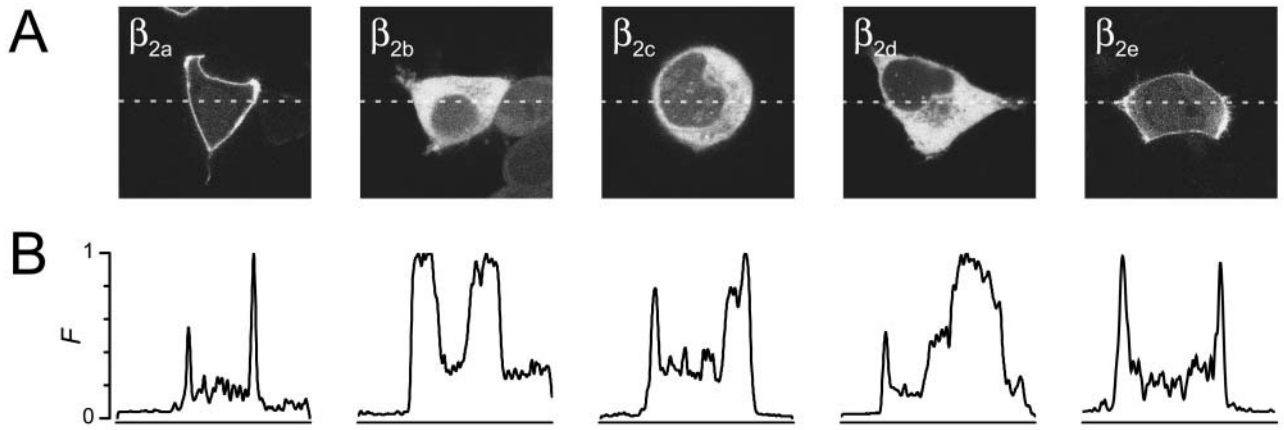

FIGURE 2 Recombinant human β_2 splice variants target differentially in HEK 293 cells. (*A*) Confocal, and (*B*) line-scan images of β_2-GFP fusion proteins. β_{2a} and β_{2e} splice variants were localized to the plasma membrane; membrane targeting of β_{2a} is caused by palmitoylation of two cysteines in D1. In contrast, β_{2b}–β_{2d} variants were distributed throughout the cytosol but excluded from the nucleus. *F* is the normalized fluorescence intensity through the midpoint of images in *A*.

tagged β_{2b}–β_{2d} proteins with an untagged Ca^{2+} channel α_{1C}-subunit did not perceptibly change their subcellular localization over that observed with the β_2-GFP subunits alone (not shown). This result might be expected given the likelihood that the β_2-subunits are overexpressed with respect to the α_1-subunit. To more directly demonstrate an interaction between our cloned β_2 variants and α_1-subunits, we turned to functional electrophysiological studies. The strict dichotomy in targeting we observed presaged functional distinctions among the β_2-splice variants as presented below.

Divergent modulatory effects of β_2-splice variants on L-type channel inactivation gating

Tuning of Ca^{2+} channel inactivation kinetics is a well-recognized and important function of auxiliary β subunits. Therefore, we investigated this dimension of β_2-splice variant function in recombinant L-type Ca^{2+} channels (α_{1C}, β_2, $\alpha_2\delta$) reconstituted in HEK 293 cells. Reconstitution of robust whole-cell Ba^{2+} currents (Figs. 3–6) amply demonstrated the viability of the cloned β_2 subunits. In the absence of co-expressed β subunits, reconstituted L-type channel currents are exceedingly small and only infrequently observed. Distinctive effects of β_2 splice variants on key L-type channel inactivation parameters were measured as described below.

Kinetics and voltage-dependence of current inactivation

With each β_2 variant, 1-s depolarizing steps to 0 mV produced L-type channel currents that activated quickly and then decayed with biexponential kinetics (Fig. 3 *A*). However, there were quantitative distinctions among the β_2 variants with regard to the degree of inactivation conferred to the channel. This effect was immediately apparent by comparing the normalized mean current waveform for β_{2a} channels with those of channels reconstituted with β_{2b}–β_{2e} subunits, respectively (Fig. 3 *A*; *gray traces* are reproductions of β_{2a} current waveform). β_{2b}–β_{2d} channels exhibited clearly faster inactivation kinetics compared to β_{2a} channels as reported visually by the discordance between corresponding current waveforms. By contrast, β_{2e} channels inactivated with virtually identical slow kinetics as β_{2a}. Hence, membrane-targeted β_2 variants (β_{2a} and β_{2e}) conferred slower inactivation kinetics compared to variants localized in the cytosol (β_{2b}–β_{2d}). This simple correlation is in accord with the notion that the characteristic slowed inactivation kinetics imparted by β_{2a} to HVA Ca^{2+} channels is due to its anchoring to the plasma membrane (Restituito et al., 2000).

We examined the voltage-dependence of channel inactivation by utilizing a family of 1-s voltage steps from −20 to +30 mV. To compare β_2-splice variant signatures on the voltage-dependence of inactivation in a straightforward manner, we used the fraction of current remaining 300 ms after depolarization (r_{300}) as an index of channel inactivation (Fig. 3 *B*). For β_{2a} channels, r_{300} values barely changed in the voltage range from −20 mV ($r_{300} = 0.70 \pm 0.03$) to +20 mV ($r_{300} = 0.64 \pm 0.03$). Continuing the trend of functional similarities between these two β_2 variants, r_{300} values for β_{2e} channels were mostly superimposed on values obtained for β_{2a} channels (Fig. 3 *B*) over this voltage range. In sharp contrast, r_{300} values for β_{2b}–β_{2d} channels dropped appreciably with increasing voltage, indicating a stronger voltage-dependence of inactivation for these channels compared to those reconstituted with β_{2a} and β_{2e}. Moreover, r_{300} values for β_{2b}–β_{2d} channels were significantly depressed compared to values obtained for β_{2a} and β_{2e} channels over a wide range of voltages, reflecting the greater rate of macroscopic current decay observed with cytoplasmically localized β_2 subunits (Fig. 3 *B*).

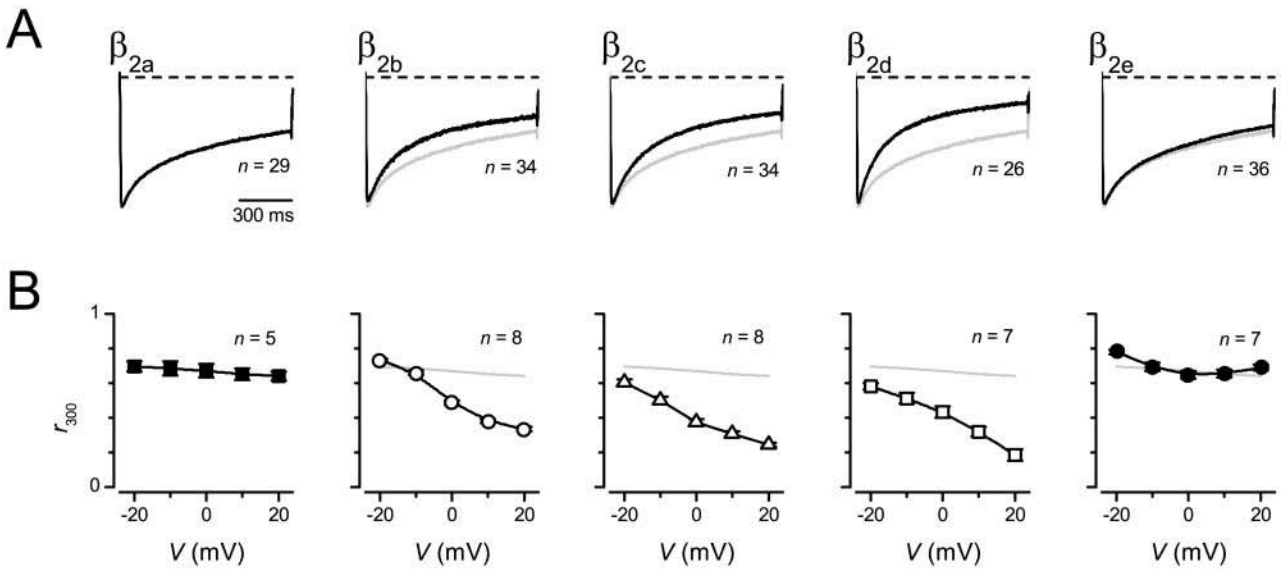

FIGURE 3 β_2 splice variants confer distinctive inactivation kinetics to recombinant L-type channels. (*A*) Normalized and averaged Ba^{2+} currents evoked by 1-s depolarizations to 0 mV. All currents had biexponential inactivation kinetics; those reconstituted with β_{2a} and β_{2e} had markedly slow inactivation kinetics compared to β_{2b}–β_{2d}. (*B*) Voltage-dependence of fast inactivation. The fraction of current remaining 300 ms into the test pulse, r_{300}, was computed as an index of inactivation. Higher r_{300} values reflect a slower rate of inactivation. Inactivation conferred by β_{2a} and β_{2e} was markedly less voltage-dependent compared to β_{2b}–β_{2d}. In both *A* and *B*, β_{2a} data are reproduced as gray lines in β_{2b}–β_{2e} panels to permit direct visual comparison.

Recovery from inactivation

Next, we investigated the effects of β_2-splice variants on the kinetics of L-type-channel recovery from inactivation. After a 1-s conditioning pulse to 0 mV, test-pulse currents recovered with biexponential kinetics for all the β_2 forms (Fig. 4). In fact, across β_2 variants, the two components of recovery from inactivation were well described as the sum of two exponential functions with identical time constants (τ_{fast} = 91.6 ms, and τ_{slow} = 20 s), but differing amplitudes (Fig. 4). Here again, there was a clear demarcation in the functional properties of membrane-bound versus cytosolic β_2 variants—β_{2a} and β_{2e} displayed a similarly lower fraction of channels recovering from inactivation with fast kinetics, compared to β_{2b}–β_{2d} channels. This is visually apparent from the virtual congruence of recovery curves between β_{2a} and β_{2e} channels, and their divergence from curves obtained with β_{2b}–β_{2d} channels (Fig. 4). Mean values of the fractional recovery from inactivation (*RF*) measured at interpulse durations of 100 ms and 4.1 s were significantly different between $\beta_{2a/e}$ and β_{2b-d} channels (RF_{100} values were: β_{2a}, 0.35 ± 0.03, n = 8; β_{2b}, 0.53 ± 0.02, n = 7; β_{2c}, 0.46 ± 0.05, n = 6; β_{2d}, 0.47 ± 0.03, n = 5; β_{2e}, 0.37 ± 0.05, n = 7; $P < 0.01$, one-way ANOVA). Our results are in qualitative agreement with previous work showing that L-type channels recover from inactivation with biexponential kinetics (Zuhlke and Reuter, 1998; Jeziorski et al., 2000). Moreover, distinct β-subunit isoforms were found to differentially modulate L-type channel recovery from inactivation (Jeziorski et al., 2000). We now show that more subtle sequence variations conferred by alternative splicing within a single β-subunit isoform are sufficient to confer differential modulation of L-type channel recovery from inactivation. The biexponential nature of the kinetics of recovery from inactivation strongly indicates the presence of two kinetically distinct forms of inactivation (Kass and Sanguinetti, 1984; Hering et al., 2000). We defer consideration of the possible physical processes underlying these forms of inactivation, and the mechanism of their differential modulation by β_2 splice variants, to the Discussion.

Steady-state inactivation

Finally, to complete our examination of modulation of L-type channel inactivation gating by β_2-splice variants, we probed quasi-steady-state inactivation (hereafter referred to as steady-state inactivation) using a three-pulse protocol in which a 10-ms prepulse to 0 mV was followed in turn by a family of 20-s conditioning pulses (−80 to +20 mV), and a 100-ms test pulse to 0 mV (Fig. 5). By contrast with the trends established above regarding clear-cut functional distinctions between membrane-bound and cytosolic β_2 variants, there were only minor distinctions in steady-state inactivation curves (Fig. 5; Table 1). All the curves were well described by single-Boltzmann functions with identical values for k, and nearly identical values for $V_{1/2}$ (Table 1). This finding is in agreement with previous studies indicating a relative resistance of L-type channel steady-state inactivation curves to manipulation by distinct Ca^{2+} channel β subunits (Jones et al., 1998). This is opposite the situation

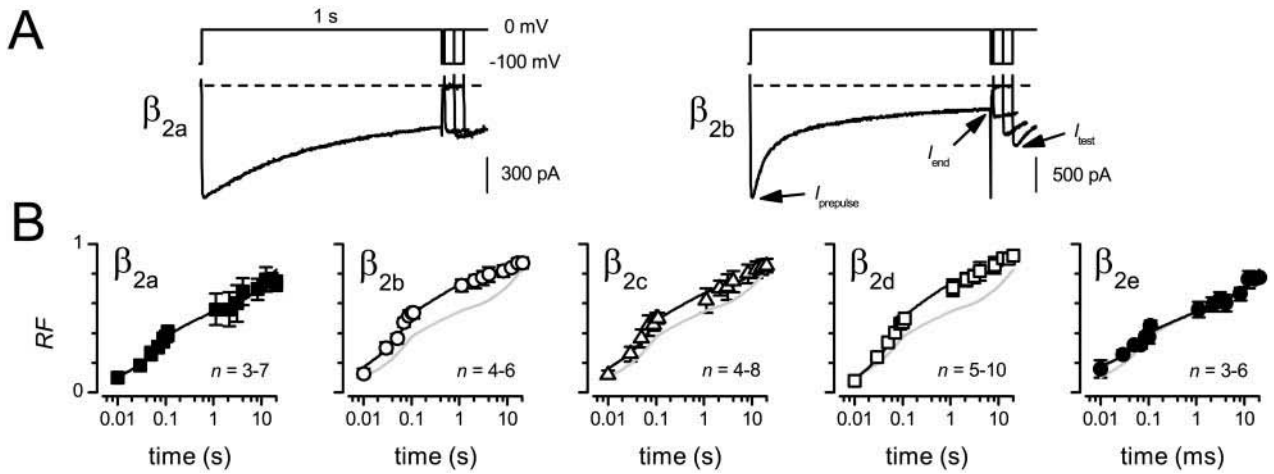

FIGURE 4 L-type channel recovery from inactivation occurs with distinct fast and slow components, but with differing amplitudes, across β_2 splice variants. (*A*) Exemplar current traces from β_{2a} and β_{2b} channels evoked by a traditional recovery from inactivation protocol in which a 1-s prepulse to 0 mV is followed by a 50-ms test pulse to 0 mV at variable interpulse durations. Here and throughout, β_{2a} and β_{2b} exemplars are shown as representative slow- and fast-inactivating channels, respectively. (*B*) Plots of the fractional recovery from inactivation, *RF*. Data points were calculated as $RF = (I_{test} - I_{end})/(I_{prepulse} - I_{end})$. Peak prepulse currents decreased by ~20% for all β_2 variants by the end of the recovery protocol. This rundown was systematically accounted for in the analysis by normalizing all currents to the peak prepulse current from the first sweep. Smooth black curves through the data are biexponential fits generated from the equation presented in Methods. Curves were constrained to have the same fast- and slow- time constants, while the amplitudes of fast and slow components were determined by least-squares criteria (parameter values are presented in Table 1). Biexponential fits to β_{2a} data are reproduced in the other panels (*gray curves*) to facilitate visual comparison of the kinetics of recovery from inactivation among the β_2 splice variants. β_{2a} and β_{2e} had a smaller fraction of channels recovering from inactivation with fast kinetics compared to β_{2b}–β_{2d} channels.

in neuronal Ca^{2+} channels (N-, P/Q- and R-type), where β-subunit identity is a major determinant of steady-state inactivation profiles (Jones et al., 1998; Stea et al., 1994).

Overall, our in-depth study of modulation of L-type channel inactivation gating by β_2 splice variants has revealed fundamental functional differences between membrane-bound (β_{2a} and β_{2e}) and cytosolic (β_{2b}–β_{2d}) β_2 subunits. Further, we find that the functional distinctions imposed by membrane-bound β_2 subunits on L-type channels are more pervasive than previously realized.

Distinctive effects of β_2-splice variants on L-type channel steady-state activation and prepulse facilitation

One prominent effect of Ca^{2+} channel β subunits is that they shift the voltage-dependence of Ca^{2+} channel activation gating in the hyperpolarizing direction. By contrast with their markedly divergent influences on channel inactivation kinetics, β subunits are traditionally viewed as having more homogeneous effects on steady-state activation profiles. Moreover, while the D1 domain of β subunits is appreciated to be an important determinant of Ca^{2+}-channel inactivation, it is presumed to play only a minor role in steady-state activation. Recently, however, alternative D1 splice variants of the β_4 subunit were found to differentially modulate the voltage-dependence of activation of N- and P/Q- type channels, thereby challenging this simple interpretation (Helton and Horne, 2002). Therefore, we investigated possible distinctions in β_2 splice variant modulation of L-type channel steady-state activation utilizing traditional tail-activation (*G-V*) protocols (Fig. 6).

To permit first-order comparison of *G-V* curve waveforms among the β_2 variants, we generated dual-Boltzmann fits by constraining $V_{1/2}$ and k values for both high- and low-threshold components, and determined the amplitudes of the two components by least-squares criteria (values in Table 1 and its legend). The impressive fits obtained for each β_2 variant authenticated this strategy (Fig. 6 *B*). Explicit overlay of the fits to data obtained from β_{2a} channels (*gray traces* in Fig. 6 *B*) onto the graphs for other splice variants provided a qualitative indication of distinctions in L-type channel steady-state activation among the different β_2 variants. Most notably, β_{2b} and β_{2e} channels displayed *G-V* curves with opposite shifts in the relative amplitude of low- versus high-threshold components compared to β_{2a} channels (Fig. 6 *B*). Specifically, whereas β_{2b} decreased the fraction of channels activating at a lower voltage threshold ($F_{low} = 0.36$ for β_{2b} versus 0.70 for β_{2a}), β_{2e} increased this parameter ($F_{low} = 0.99$). By contrast, β_{2c} and β_{2d} channels displayed *G-V* curves that were relatively unchanged, or only subtly different from β_{2a} (Fig. 6 *B*). These results revealed an unappreciated role of the D1 domain of Ca^{2+}-channel β_2 subunits as an important determinant of L-type channel steady-state activation gating in addition to their more recognized function in modulating inactivation. The distinctions in activation gating did not extend to the kinetics of channel activation, as single exponential fits to the activation phase of currents

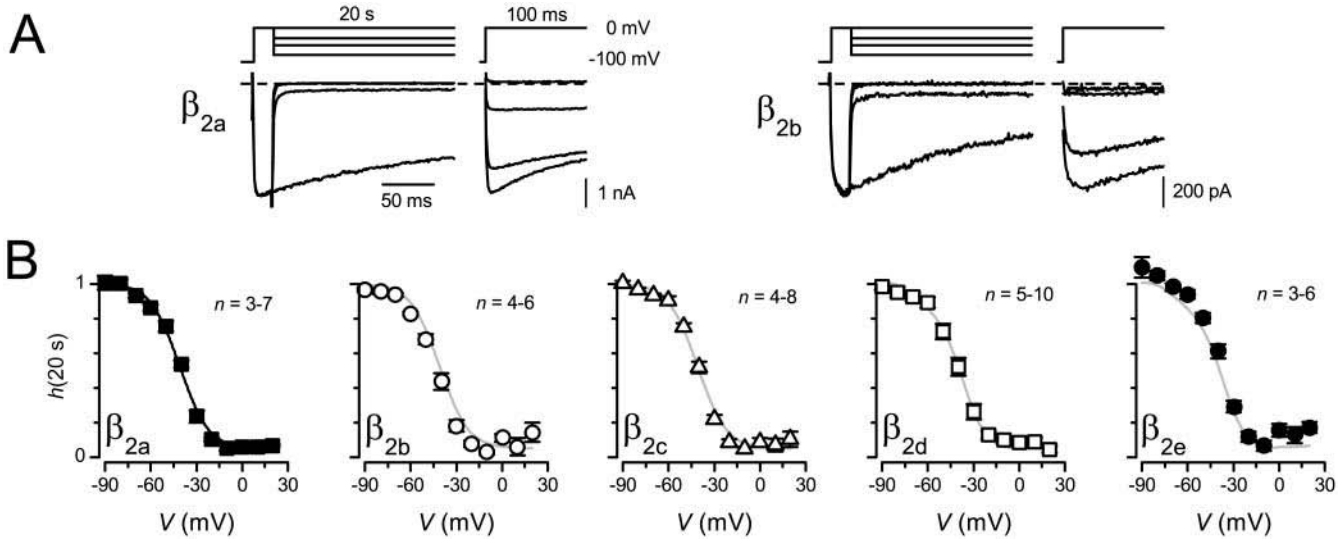

FIGURE 5 L-type channel steady-state inactivation properties are relatively insensitive to the identity of the component β_2-subunit splice variant. (*A*) Exemplar current traces from β_{2a} and β_{2b} channels evoked by a traditional steady-state inactivation protocol in which a 10-ms normalizing pulse to 0 mV is followed sequentially by a variable-voltage family of 20-s conditioning pulses and a 100-ms test pulse to 0 mV. Only the first 200 ms of the currents during the conditioning depolarizations is shown. Traces shown were obtained with conditioning pulse voltages of 0, −30, −50, and −80 mV. (*B*) Plots of steady-state inactivation, $h(20\ s)$, as a function of voltage of the conditioning pulse. The normalized data points were obtained from the peak values of the prepulse and test currents, repectively, as $h(20\ s) = I_{test}/I_{prepulse}$. Smooth black curve through the β_{2a} data was generated from a single Boltzmann function as described in Methods, with parameter values given in Table 1. Reproduction of the β_{2a} Boltzmann fit onto the panels for other β_2 splice variants (*gray curves*) demonstrated marked agreement with these other data, indicating little difference among the distinct β_2 variants.

evoked by 0-mV test pulses produced time constants that were not significantly different among the β_2 variants (not shown).

A potential explanation (suggested by reviewers) for the increasing activation observed at positive voltages, evident as the high-threshold component of *G-V* curves (Fig. 6 *B*), could be voltage-dependent facilitation of L-type channels. If so, then the distinct β_2 variants might be expected to differentially modulate this physiologically important property of L-type Ca^{2+} channels. This proposal was directly tested using a protocol in which test-pulse currents at a family of voltages were recorded with or without a 50-ms prepulse to +100 mV (Fig. 7 *A*). An interpulse duration of 50 ms at −100 mV was chosen, being long enough to ensure complete deactivation of channels after the prepulse, but short enough that any facilitation that was evoked by the prepulse would not have completely decayed. Exemplar currents evoked from β_{2a} and β_{2b} channels both displayed prepulse facilitation, although to different extents (Fig. 7). The larger degree of L-type channel facilitation conferred by β_{2b} resulted in a more dramatic prepulse-induced hyperpolarizing shift in the *G-V* curve for β_{2b} compared to β_{2a} (Fig. 7 *B*), fitting with the suggestion that differences in voltage-dependent facilitation may play a role in establishing the observed distinctions in waveforms of steady-state activation curves (Fig. 6). Explicit comparison of L-type channel facilitation across all five β_2-splice variants revealed that, compared to β_{2a}, only β_{2b} supported a significantly higher degree of facilitation (23.9 ± 4.8%, $n = 8$ for β_{2b}; 10.4 ± 2.5%, $n = 9$ for β_{2a}; $P < 0.05$, two-tailed Student's unpaired *t*-test; see also Fig. 7 *C*). Although β_{2d} supported a high mean value of facilitation (28.4 ± 9.7%, $n = 8$), primarily due to a single cell that exhibited an unusually large degree of facilitation (86%), this value fell short of significance when compared to β_{2a} ($P = 0.08$, two-tailed Student's unpaired *t*-test).

Overall, these results demonstrate that the D1 domain of the Ca^{2+} channel β_2 subunit is an important determinant of prepulse facilitation of L-type channels, in agreement with previous observations (Cens et al., 1998; Qin et al., 1998). However, we did not observe a strict segregation of the degree of L-type channel facilitation according to whether the supporting β_2 subunit was membrane-bound (β_{2a}, β_{2e}) or localized to the cytosol (β_{2b}–β_{2d}). Such a result might have been envisioned given a previous report that the lower degree of facilitation conferred by β_{2a} compared to other β-subunit isoforms was completely accounted for by the posttranslational palmitoylation of β_{2a} (which confines it to the membrane; see Qin et al., 1998). Hence, our results indicate that the role of the β_2-subunit D1 domain in specifying L-type channel prepulse facilitation may be more complicated than previously suspected.

DISCUSSION

The important findings presented in this study are: 1), human genomic sequence analyses permitted, for the first time, the cloning of five distinct amino-terminal β_2-subunit variants

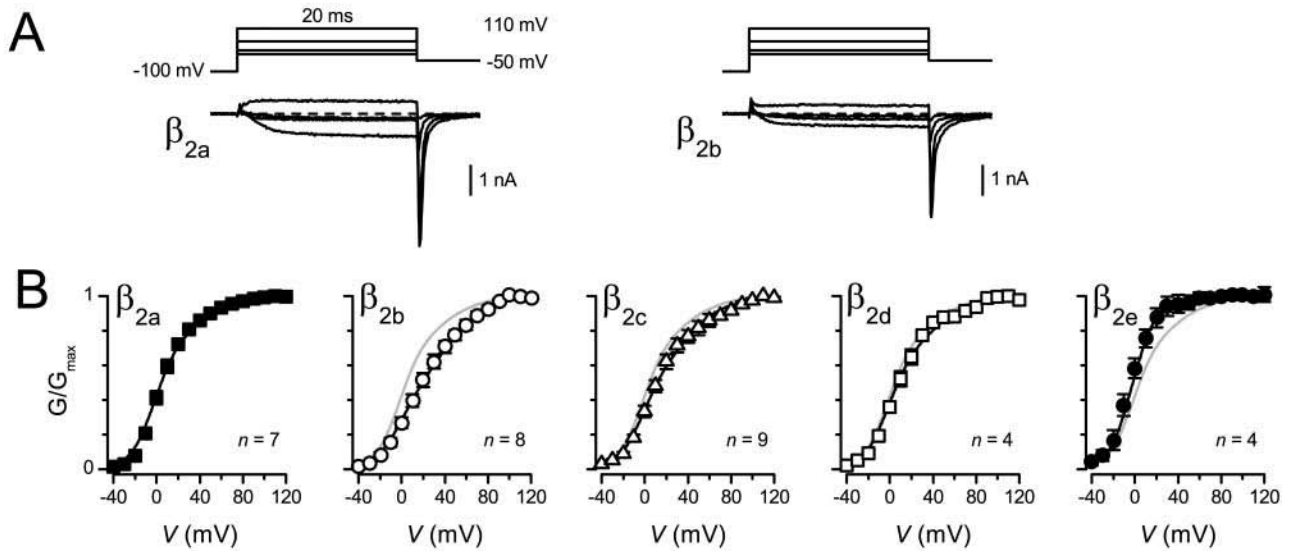

FIGURE 6 Different β_2 splice variants impart distinctive steady-state activation behavior to L-type channels. (*A*) Exemplar current traces from β_{2a} and β_{2b} channels evoked by a traditional tail-activation protocol in which channels were steady-state activated by a variable-voltage family of 20-ms test pulses, and tail currents measured after repolarization to −50 mV. Traces shown were obtained with test-pulse voltages of −20, 0, +40, and +100 mV. (*B*) Normalized (G/G_{max}) *G-V* curves for channels incorporating the different β_2 variants. Smooth black curves through the data were generated from dual-Boltzmann functions as described in Methods, with parameter values given in Table 1. To generate fits, $V_{1/2}$ and k values were constrained to the values given in the legend to Table 1, and the amplitudes of the low- and high-threshold components determined by least-squares criteria. The reproduced fits from β_{2a} data (*gray curves*) displayed varying degrees of difference from the data for other β_2 variants, visually affirming that distinct β_2 variants gave rise to differing fractions of channels that operated in the low threshold of activation regime.

from the same species, unambiguously identifying them as genuine splice variants of the β_2 gene, *CACNB2*. 2), A second β_2-subunit variant, β_{2e}, targeted unexpectedly to the plasma membrane when expressed in HEK 293 cells, in a manner akin to that previously described for β_{2a}. 3), The subcellular localization of the β_2-subunit forms was correlated with the kinetics of L-type current decay—membrane-anchored subunits (β_{2a} and β_{2e}) produced slowly inactivating currents, whereas cytoplasmic subunits (β_{2b}–β_{2d}) imparted relatively faster inactivation kinetics. 4), For all subunit combinations, L-type channels displayed a biexponential recovery from inactivation. However, membrane-anchored β_{2a} and β_{2e} channels exhibited a smaller fraction of channels recovering with fast kinetics compared to their cytosol-localized counterparts. 5), L-type channel steady-state activation curves displayed low- and high-threshold components with distinct β_2 splice variants differentially determining the relative amplitudes of the two components. 6), The distinct β_2 variants supported varying degrees of prepulse facilitation of L-type channels.

We discuss these results in relation to previous studies in terms of their biophysical and physiological implications.

Historical perspective on cloning and nomenclature of Ca^{2+} channel β_2-subunit splice variants

The first Ca^{2+} channel β_2 subunit was cloned from rat brain (Perez-Reyes et al., 1992) and has commonly been referred to as β_{2a}. Shortly thereafter, two β_2-subunit homologs were cloned from rabbit heart (Hullin et al., 1992). These differed from each other and from the rat brain β_{2a} subunit only in the amino-terminal D1 domain, all other parts of the proteins being essentially identical. Nevertheless, the rabbit clones were dubbed rabbit β_{2a} and rabbit β_{2b}. A fourth β_2 variant with a unique D1 domain was subsequently cloned from human fetal brain (Rosenfeld et al., 1993) and is commonly referred to as β_{2c}. Finally, a fifth β_2 subunit with a distinctive D1 domain was cloned from mouse brain and was originally denoted as mouse brain β_{2a} (Massa et al., 1995), although this variant has more recently been referred to as β_{2d} (Yamaguchi et al., 2000). Before the present study, no more than three of the β_2 forms had been cloned from any one species, making it uncertain whether all five were genuine splice variants, or simply reflected species variation. Recently, based on human genome sequence analysis, we reported that all five described β_2 D1 domains were represented within the human β_2 gene (Colecraft et al., 2002). Here, by cloning all five β_2 forms from human cDNA libraries, we explicitly confirm their collective expression in a single species, unequivocally establishing that they are true splice variants. This insight validates our proposal to rename the five distinct β_2 D1 variants β_{2a}–β_{2e} (Colecraft et al., 2002), as we have adopted in this study.

The fragmentary nature of the history of discovery of the distinct β_2 variants can be attributed to limitations in traditional cloning methods, which rarely provide an exhaustive representation of splice variants within a given gene. The

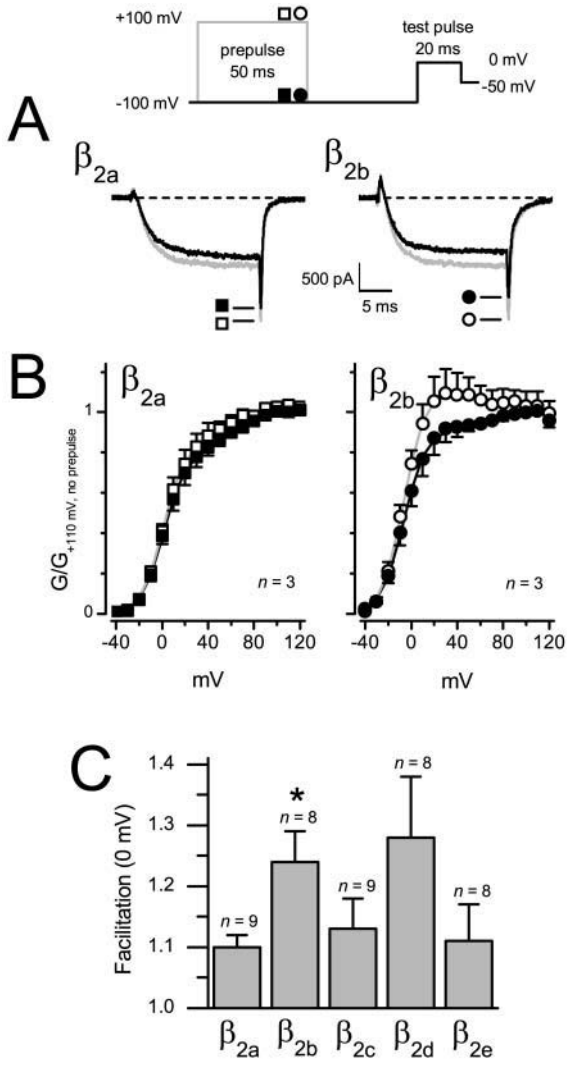

FIGURE 7 β_2 splice variants differentially affect prepulse facilitation of recombinant L-type channels. (*A*) Alternating prepulse voltage protocol (*above*) and exemplar Ba^{2+} test-pulse currents (*below*) recorded from L-type channels reconstituted with β_{2a} (*left*) or β_{2b} (*right*). Currents were evoked by a 20-ms test-pulse to 0 mV in the absence of prepulse (*black traces*) or after a 50-ms prepulse to +100 mV (*gray traces*); the interpulse duration was 50 ms. Tail currents were analyzed at −50 mV repolarization potential. (*B*) Normalized and averaged *G-V* curves generated from alternating-prepulse protocol for L-type channels reconstituted with β_{2a} (*left*, ■, □) and β_{2b} (*right*, ●, ○). Tail-current amplitudes were normalized to the current evoked at +110 mV in the absence of prepulse and plotted as a function of test-pulse potential, which was varied from –40 to +120 mV in 10-mV increments. Solid symbols (■, ●) denote currents evoked in the absence of prepulse; open symbols (□, ○) denote currents evoked after a prepulse. (*C*) Comparison of facilitation measured at a test-pulse potential of 0 mV across all five β_2 splice variants. Facilitation was calculated as the tail-current amplitude after a prepulse, normalized to the tail-current amplitude in the absence of prepulse. The difference between β_{2a} and β_{2b} was statistically significant (asterisk denotes $P < 0.05$, Student's *t*-test).

availability of the human genome sequence, and other ongoing mammalian genome sequencing efforts, provides a more panoramic perspective from which to study molecular diversity generated by alternative splicing. Genomic sequence information is particularly advantageous in identifying splice variants with different first or last exons. By contrast to splice variations that occur in internal exons, such first- and last-exon splice variants cannot be isolated by the technique of transcript-scanning PCR (Mittman et al., 1999). Overall, our study powerfully demonstrates the advantages of genome-based cloning over more traditional methods in identifying and cloning alternative splice variants of a gene.

Importance of Ca^{2+} channel β-subunit subcellular localization

Hydropathy analysis indicates a lack of membrane-spanning domains in Ca^{2+}-channel β subunits (Perez-Reyes et al., 1992; Castellano et al., 1993a), predicting that they would localize to the cytosol when expressed in cells. This prediction is met for the majority of Ca^{2+}-channel β subunits so far examined. However, β_{2a} bucked this trend when it was discovered that it targeted to the plasma membrane when exclusively expressed in HEK 293 cells (Chien et al., 1995). Subsequently, this anomalous localization was attributed to palmitoylation of β_{2a}, in perfect agreement with the identification of a consensus motif for such modification in the amino terminus of the protein (Milligan et al., 1995; Chien et al., 1996; Resh, 1999). Importantly, such membrane localization of β_{2a} has been associated with a constellation of distinguishing functional effects including: slowing of Ca^{2+}-channel inactivation kinetics (Qin et al., 1998; Restituito et al., 2000); depolarizing shifts in the voltage-dependence of steady-state inactivation in neuronal Ca^{2+} channels (Jones et al., 1998); abolition of voltage-dependent facilitation of L-type channels expressed in *Xenopus* oocytes (Qin et al., 1998); and modulation of G-protein inhibition of neuronal Ca^{2+} channels (Qin et al., 1997). Hence, the subcellular location of β subunits is an important determinant of function.

Here, we have identified β_{2e} as a second β_2 splice variant that targets anomalously to the plasma membrane when expressed alone in HEK 293 cells. The mechanism underlying β_{2e} targeting to the membrane is unclear, although the molecular determinants of this localization must reside in its unique D1 domain. Unlike β_{2a}, visual inspection of the β_{2e} D1 domain does not immediately reveal likely sites for posttranslational lipid modification (Milligan et al., 1995; Resh, 1999). Further work will be needed to delineate the mechanism of β_{2e} targeting to the membrane. Interestingly, β_{2a} and β_{2e} were functionally similar, lending support to the hypothesis that physical association with the membrane underlies the characteristic effects of β_{2a} on Ca^{2+} channels (Restituito et al., 2000). The Ca^{2+}-channel β_{1b} subunit has also been reported to be membrane-localized when expressed in COS-7 cells (Brice et al., 1997) due to an acidic motif in the carboxyl terminus of the protein (Bogdanov et al., 2000). However, this property is not reproduced in other cell types (Chien et al., 1998; Colecraft et al., 2002) and does not result in any distinguishing electrophysiolog-

ical phenotypes (Bogdanov et al., 2000). Hence, β_{2a} and β_{2e} are, thus far, clearly unique in this regard.

Our results contribute to a growing awareness that the subcellular distribution of Ca^{2+}-channel subunits represents an important dimension of their function (Brice and Dolphin, 1999; Colecraft et al., 2002). The approach of viewing such distribution by tagging subunits with GFP is useful for such studies and offers the distinct advantages of: 1), permitting viewing of subunit localization in living cells, and 2), avoiding artifacts due to inaccessibility of epitopes or nonspecificity of antibodies. Indeed, we recently used this approach to reveal unexpected targeting of β_4 subunits to the nucleus and transverse elements when expressed in heart cells (Colecraft et al., 2002). Nevertheless, the results of such experiments need to be interpreted with caution because of potential confounding factors arising from fusion of the relatively large GFP molecule to the target protein. For example, fusion of GFP to the amino-terminus of β_{2a} abolishes membrane targeting, presumably by interfering with the palmitoylation of the cysteine residues in this region (H. M. Colecraft, unpublished observations).

Quantitative mechanism of β_2-subunit modulation of L-type channel inactivation gating

L-type Ca^{2+} channels undergo at least three types of inactivation—Ca^{2+}-dependent inactivation, and fast and slow forms of voltage inactivation. Ca^{2+}-dependent inactivation is mediated by binding of Ca^{2+} to calmodulin that is tethered to the channel complex (Peterson et al., 1999; Qin et al., 1999; Zuhlke et al., 1999; Erickson et al., 2001; Pitt et al., 2001) and displays a characteristic ''U-shaped'' response to voltage that is a direct reflection of its current dependence. Our use of Ba^{2+} as charge carrier eliminates Ca^{2+}-dependent inactivation; therefore, we will consider this form of inactivation no further. Instead, under our experimental conditions, fast and slow forms of voltage-dependent inactivation are prevalent. Mechanistically, it has been speculated that fast inactivation of HVA Ca^{2+} channels may be analogous to fast N-type inactivation in K^+ channels (Hoshi et al., 1990; Zagotta et al., 1990) and to the fast hinged-lid inactivation mechanism in Na^+ channels (West et al., 1992), both of which involve physical occlusion of the pore by cytoplasmic domains of the channel (Hering et al., 2000; Stotz and Zamponi, 2001). A leading candidate for the tethered plug in HVA Ca^{2+} channels is the cytoplasmic loop between domains I and II (I–II loop; Cens et al., 1999b; Stotz et al., 2000; Stotz and Zamponi, 2001), although the possible existence of inactivation gates on other parts of the pore-forming α_1 subunit, or accessory β subunits, has not been excluded. Similarly, slow inactivation of Ca^{2+} channels may be analogous to C-type inactivation of K^+ channels (Shi and Soldatov, 2002), which involves a constriction of the channel pore (Choi et al., 1991; Kukuljan et al., 1995). Here, the biexponential kinetics of current decay and recovery from inactivation authenticated the prevalence of both fast and slow inactivation across all five β_2-splice variants. Nevertheless, there were key distinctions in L-type channel gating that segregated into two categories, depending on whether the associated β_2 subunit was membrane-anchored, or localized in the cytosol. Specifically, membrane-anchored β_2 subunits (β_{2a} and β_{2e}) produced a slower rate of channel inactivation (Fig. 3 *A*), exhibited elevated r_{300} values over the range of voltages (Fig. 3 *B*), and displayed a smaller fraction of channels with fast recovery from inactivation kinetics (Fig. 4). By contrast, steady-state inactivation was not very different among distinct β_2 variants (Fig. 5).

To gain mechanistic insights into the variable effects of β_2 variants on L-type channel inactivation gating, we turned to quantitative modeling (Fig. 8). Since inactivation characteristics conferred by the β_2 variants segregated into two major divisions, we modeled β_{2a} and β_{2b} channels as representatives of the two functional phenotypes. As a starting point, the biexponential kinetics of recovery from inactivation suggested two kinetically distinct inactivation states. Therefore, we first considered alternative schemes that could give rise to such behavior. In this regard, a three-state model consisting of one open and two inactive states was recently invoked to explain the biexponential kinetics of inactivation and recovery in recombinant P/Q-type Ca^{2+} channels (Sokolov et al., 2000; Berjukow et al., 2001). In those studies, inactivation from the open state could occur by two separate pathways with either a fast or slow rate. By itself, this minimal three-state model cannot describe features such as the voltage-dependence of inactivation or steady-state inactivation. Therefore, we incorporated the three-state inactivation mechanism into a modified Hodgkin-Huxley kinetic model (Fig. 8 *A*, Scheme 1), similar in structure to those previously used for voltage-gated K^+ (Zagotta and Aldrich, 1990), Na^+ (Armstrong and Bezanilla, 1977), and Ca^{2+} channels (Boland and Bean, 1993; Colecraft et al., 2002). Here, the activation pathway consisted of three voltage-dependent transitions ($C \rightarrow C$) followed by a distinct voltage-independent step immediately preceding channel opening ($C \rightarrow O$). Transitions from the activation pathway to the inactive states were state-dependent but voltage-independent; allosteric inactivation and recovery factors, f and h, respectively, served to hasten inactivation from the open state and enhance recovery to closed states (Klemic et al., 1998; Serrano et al., 1999). Additionally, inactive states were separated into those connected to the activation pathway with either fast or slow entry/exit rates (I_f and I_s respectively). Although simulations using Fig. 8 *A*, Scheme 1 could qualitatively predict aspects of the inactivation properties conferred by β_2 splice variants, quantitative agreement with experimental data was elusive (simulations not shown). Moreover, it proved difficult to obtain simultaneous good fits to inactivation and recovery kinetics.

Consequently, we considered a second scheme that could describe the biexponential behavior of L-type channel inactivation and recovery from inactivation kinetics. Such

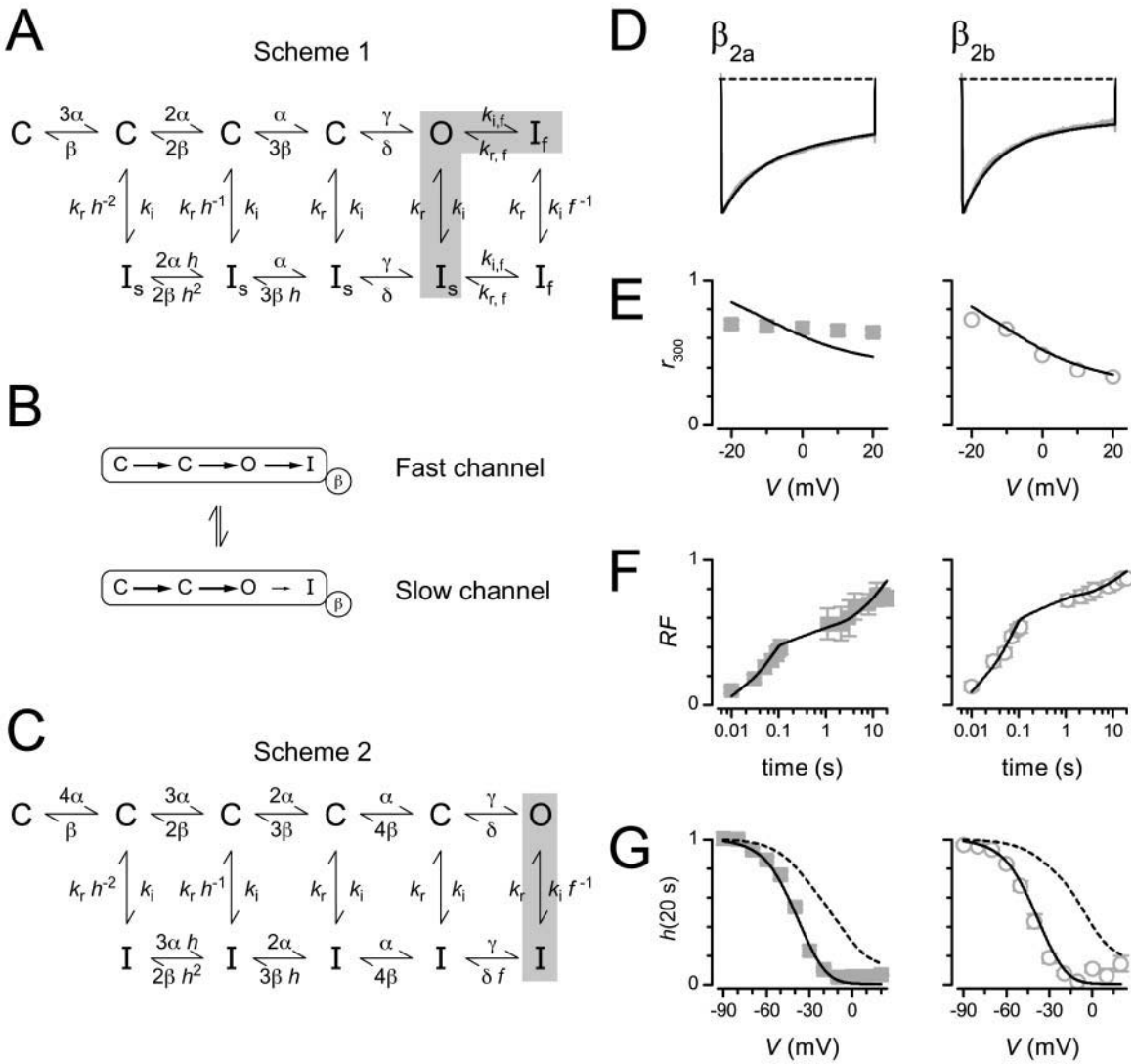

FIGURE 8 Quantitative descriptions of L-type channel inactivation gating profiles as conferred by distinct β_2 splice variants. (*A–C*) Alternative kinetic schemes that could account for the existence of two kinetically distinct inactivation states, which are suggested experimentally by the biexponential kinetics of channel recovery from inactivation. In Fig. 8 *A*, Scheme 1, inactive states were separated into those connected to the activation pathway with either fast or slow entry/exit rates (I_f and I_s, respectively). In Fig. 8 *C*, Scheme 2, inactivation proceeds from the open state by only one pathway. In this case, the biexponential kinetics of recovery from inactivation arise from the existence of two channel populations (or modes) displaying kinetically distinct fast and slow modes of inactivation. (*D–F*) Simulations of inactivation gating of β_{2a} and β_{2b} channels using Fig. 8 *C*, Scheme 2 showed marked agreement between the model (*black curves*) and experimental data (*gray curves*, and ■, ○). Values of rate constants used in simulations are presented in Table 2. In simulations, the fraction of fast channels was given by the corresponding F_{fast} values, as determined from recovery from inactivation protocols (Table 2). Note that for simulations of β_{2a} and β_{2b} channels, rate constants were identical in the two cases. Hence, all the differences between the channel types were completely accounted for by the differing values of the fraction of fast inactivating channels, F_{fast}. (*G*) In the case of steady-state inactivation, simulations using the dual-population model as described above (*dotted lines*) diverged from the experimental data (■, ○). Remarkably, when it was assumed that all the channels were gating in the slow mode, model predictions of steady-state inactivation (*black curves*) superimposed the experimental data. This suggested that during the ultra-long 20-s conditioning pulses used in steady-state inactivation protocols, channels consolidate into the slow inactivating mode. Evidence of such consolidation has been experimentally observed.

behavior could arise from the existence of two channel populations displaying kinetically distinct fast and slow modes of inactivation (Fig. 8 *B*). To implement this dual-population scenario, fast and slow channels were both simulated independently using a modified Hodgkin-Huxley model (Fig. 8 *C*, Scheme 2). In contrast to Scheme 1, Fig. 8 *A*, inactivation could occur from the open state by only one pathway. Biexponential recovery-from-inactivation kinetics emerged from the existence of fast and slow channel populations rather than two exit pathways from the open state. For simplicity, the fast and slow channels employed identical rate parameters except for the microscopic inactivation rate constants k_i and k_r (Table 2). To simulate β_2-subunit-specific effects on inactivation gating by this scheme, we set

the fraction of fast channels to be the corresponding F_{fast} values calculated from recovery from inactivation protocols (Table 1) and computed the total current as the weighted sum of fast and slow channels.

This strategy furnished a strong agreement between model simulations and experimental data for inactivation and recovery kinetics (Fig. 8, *D* and *F*), a clear improvement over fits generated with Scheme 1. Less impressive initially was the fit to steady-state inactivation data generated by the model (Fig. 8 *G*, *dotted trace*). Remarkably, however, the model produced steady-state inactivation curves congruent with experimental data when it was assumed that all the channels were in the slow-inactivating mode (Fig. 8 *G*, *solid curve*). This finding suggested that over the exceptionally long 20-s prepulse duration employed to generate steady-state inactivation curves, initially fast-inactivated channels are consolidated into a slow-inactivated mode. In fact, such consolidation with increasingly prolonged depolarizations has been experimentally observed (Sokolov et al., 2000). For voltage-dependence of inactivation, simulations showed qualitative agreement, although they predicted a steeper voltage-dependence of r_{300} for β_{2a} than was experimentally determined (Fig. 8 *E*). This discordance may indicate that β_{2a} may act to slow the microscopic propensity for inactivation in fast channels. Such a scenario would be consistent with the conceptualization that membrane tethering of β_{2a} would serve to slow the rate of engagement of an inactivation gate (presumably the α_1-subunit cytoplasmic I–II loop) with its receptor site (Restituito et al., 2000; Stotz and Zamponi, 2001). Such predictions could be tested within the framework of the currently proposed model.

Overall, the differing effects of β_2 variants on L-type channel inactivation gating are well described by a model in which L-type channels distribute reversibly between fast and slow inactivating modes, with membrane-bound β_2 forms displaying an ~50% lower fraction of fast channels compared to cytosolic β_2 subunits. At the single-channel level, fast and slow channels may be equivalent to the rapidly and slowly inactivating modes observed in N-type channels recorded from rat superior cervical ganglion neurons (Plummer and Hess, 1991). Finally, although this model is preliminary, since rate parameters were determined empirically and we have not systematically ruled out alternative models, it provides a framework for the design of future experiments aimed at investigating mechanisms of channel gating (Serrano et al., 1999).

Possible physiological implications of β_2-subunit splice variation

Beyond the biophysical implications discussed above, our results also raise issues of physiological importance. First, Ca^{2+} currents recorded from many native preparations frequently display a slower inactivating phenotype than expected. It is often tacitly assumed that such behavior may indicate an association of the α_1 subunit with β_{2a}. Our results indicate that this interpretation is not necessarily correct. Here, we identify β_{2e} as a second β_2-splice variant that gives rise to comparably slow currents as β_{2a}. This finding gives reason to wonder whether there are as-yet-unidentified membrane-bound splice variants of other β-subunit isoforms present in native cells. Such subunits could potentially also give rise to slow inactivating currents upon association with native α_1 subunits. Our studies provide a firm foundation to investigate this intriguing notion.

Second, our results indicate that alternatively spliced β_2 subunits would be expected to differentially tune critical functional properties of native voltage-dependent Ca^{2+} channels ranging from modulation of inactivation kinetics to determining the extent of prepulse facilitation. The influence of such β_2-subunit splice variation would be expected to be especially significant in tissues or cells in which β_2 is the sole or predominant β subunit, as is the case in heart (Perez-Reyes et al., 1992; Colecraft et al., 2002) and outer plexiform layer of the retina (Ball et al., 2002). Different β_2-splice variants have been identified in heart cDNA libraries from different species (Hullin et al., 1992; Yamada et al., 2001; Colecraft et al., 2002), raising the possibility that multiple β_2-splice variants exist either in single heart cells, or in cells from different regions of the heart. Our results predict this would lead to functionally heterogeneous L-type channels in heart, with possible implications for cardiac function. Further studies are required to explore such physiological dimensions of β_2-subunit splice variation.

A full appreciation of the likely physiological impact of β_2-subunit splice variation must await studies determining the relative expression levels and tissue distributions of the different β_2 forms. Such studies would benefit from the isolation of the full complement of β_2 splice variants in other mammalian species from which cells and tissue would be more readily available. To this end, we have recently used a genome-based cloning approach to amplify the rat orthologs of β_{2a}–β_{2e} subunits, two of which were previously undescribed (F. Chan and H. Colecraft, unpublished data).

CONCLUSIONS

Much work has focused on the use of artificially constructed chimeras to study the structure function of Ca^{2+}-channel β subunits (Olcese et al., 1994; Cens et al., 1998, 1999a). Molecularly diverse β subunits generated by alternative splicing constitute a potential treasure trove to gain new insights into the structure-function of α_1–β-subunit interactions and the full scope of β-subunit functions in vivo. Furthermore, studies of such natural chimeras have the added benefit of direct physiological relevance. To these ends, the availability of the human and other mammalian genomic sequences in public databases represents a key enabling asset as demonstrated in this work.

We thank David T. Yue, Michael G. Erickson, and Jenafer Evans for critical comments on the manuscript.

This work was supported by a grant from the National Institutes of Health (ROI HL-69911) to H.M.C., and a Medical Scientist Training Program Fellowship to S.X.T.

REFERENCES

Alseikhan, B. A., C. D. DeMaria, H. M. Colecraft, and D. T. Yue. 2002. Engineered calmodulins unmask prominence of Ca channels in controlling heart excitation. *Proc. Natl. Acad. Sci. USA.* 99:17185–17190.

Armstrong, C. M., and F. Bezanilla. 1977. Inactivation of the sodium channel. II. Gating current experiments. *J. Gen. Physiol.* 70:567–590.

Ball, S. L., P. A. Powers, H. S. Shin, C. W. Morgans, N. S. Peachey, and R. G. Gregg. 2002. Role of the β_2 subunit of voltage-dependent calcium channels in the retinal outer plexiform layer. *Invest. Ophthalmol. Vis. Sci.* 43:1595–1603.

Berjukow, S., R. Marksteiner, S. Sokolov, R. G. Weiss, E. Margreiter, and S. Hering. 2001. Amino acids in segment IVS6 and β-subunit interaction support distinct conformational changes during Ca(v)2.1 inactivation. *J. Biol. Chem.* 276:17076–17082.

Birnbaumer, L., N. Qin, R. Olcese, E. Tareilus, D. Platano, J. Costantin, and E. Stefani. 1998. Structures and functions of calcium channel β subunits. *J. Bioenerg. Biomembr.* 30:357–375.

Bogdanov, Y., N. L. Brice, C. Canti, K. M. Page, M. Li, S. G. Volsen, and A. C. Dolphin. 2000. Acidic motif responsible for plasma membrane association of the voltage-dependent calcium channel β_{1b} subunit. *Eur. J. Neurosci.* 12:894–902.

Boland, L. M., and B. P. Bean. 1993. Modulation of N-type calcium channels in bullfrog sympathetic neurons by luteinizing hormone-releasing hormone: kinetics and voltage dependence. *J. Neurosci.* 13: 516–533.

Brice, N. L., N. S. Berrow, V. Campbell, K. M. Page, K. Brickley, I. Tedder, and A. C. Dolphin. 1997. Importance of the different β subunits in the membrane expression of the α_{1A} and α_2 calcium channel subunits: studies using a depolarization-sensitive α_{1A} antibody. *Eur. J. Neurosci.* 9:749–759.

Brice, N. L., and A. C. Dolphin. 1999. Differential plasma membrane targeting of voltage-dependent calcium channel subunits expressed in a polarized epithelial cell line. *J. Physiol.* 515:685–694.

Brody, D. L., P. G. Patil, J. G. Mulle, T. P. Snutch, and D. T. Yue. 1997. Bursts of action potential waveforms relieve G-protein inhibition of recombinant P/Q-type Ca^{2+} channels in HEK 293 cells. *J Physiol.* 499:637–644.

Cahill, A. L., J. H. Hurley, and A. P. Fox. 2000. Coexpression of cloned α_{1B}, β_{2a}, and $\alpha_2\delta$ subunits produces non-inactivating calcium currents similar to those found in bovine chromaffin cells. *J. Neurosci.* 20:1685–1693.

Castellano, A., X. Wei, L. Birnbaumer, and E. Perez-Reyes. 1993a. Cloning and expression of a neuronal calcium channel β subunit. *J. Biol. Chem.* 268:12359–12366.

Castellano, A., X. Wei, L. Birnbaumer, and E. Perez-Reyes. 1993b. Cloning and expression of a third calcium channel β subunit. *J. Biol. Chem.* 268:3450–3455.

Catterall, W. A. 2000. Structure and regulation of voltage-gated Ca^{2+} channels. *Annu. Rev. Cell Dev. Biol.* 16:521–555.

Cens, T., S. Restituito, and P. Charnet. 1999a. Regulation of Ca-sensitive inactivation of a L-type Ca^{2+} channel by specific domains of β subunits. *FEBS Lett.* 450:17–22.

Cens, T., S. Restituito, S. Galas, and P. Charnet. 1999b. Voltage and calcium use the same molecular determinants to inactivate calcium channels. *J. Biol. Chem.* 274:5483–5490.

Cens, T., S. Restituito, A. Vallentin, and P. Charnet. 1998. Promotion and inhibition of L-type Ca^{2+} channel facilitation by distinct domains of the subunit. *J. Biol. Chem.* 273:18308–18315.

Chien, A. J., K. M. Carr, R. E. Shirokov, E. Rios, and M. M. Hosey. 1996. Identification of palmitoylation sites within the L-type calcium channel β_{2a} subunit and effects on channel function. *J. Biol. Chem.* 271:26465–26468.

Chien, A. J., T. Gao, E. Perez-Reyes, and M. M. Hosey. 1998. Membrane targeting of L-type calcium channels. Role of palmitoylation in the subcellular localization of the β_{2a} subunit. *J. Biol. Chem.* 273:23590–23597.

Chien, A. J., X. Zhao, R. E. Shirokov, T. S. Puri, C. F. Chang, D. Sun, E. Rios, and M. M. Hosey. 1995. Roles of a membrane-localized β subunit in the formation and targeting of functional L-type Ca^{2+} channels. *J. Biol. Chem.* 270:30036–30044.

Choi, K. L., R. W. Aldrich, and G. Yellen. 1991. Tetraethylammonium blockade distinguishes two inactivation mechanisms in voltage-activated K^+ channels. *Proc. Natl. Acad. Sci. USA.* 88:5092–5095.

Colecraft, H. M., B. Alseikhan, S. X. Takahashi, D. Chaudhuri, S. Mittman, V. Yegnasubramanian, R. S. Alvania, D. C. Johns, E. Marban, and D. T. Yue. 2002. Novel functional properties of Ca^{2+} channel β subunits revealed by their expression in adult rat heart cells. *J. Physiol.* 541:435–452.

Collin, T., J. J. Wang, J. Nargeot, and A. Schwartz. 1993. Molecular cloning of three isoforms of the L-type voltage-dependent calcium channel β subunit from normal human heart. *Circ. Res.* 72:1337–1344.

Colquhoun, D., and A. G. Hawkes. 1981. On the stochastic properties of single ion channels. *Proc. R. Soc. Lond. B Biol. Sci.* 211:205–235.

Davis, L. I. 1995. The nuclear pore complex. *Annu. Rev. Biochem.* 64:865–896.

De Waard, M., and K. P. Campbell. 1995. Subunit regulation of the neuronal α_{1A} Ca^{2+} channel expressed in *Xenopus* oocytes. *J. Physiol.* 485:619–634.

De Waard, M., M. Pragnell, and K. P. Campbell. 1994. Ca^{2+} channel regulation by a conserved β subunit domain. *Neuron.* 13:495–503.

Erickson, M. G., B. A. Alseikhan, B. Z. Peterson, and D. T. Yue. 2001. Preassociation of calmodulin with voltage-gated Ca^{2+} channels revealed by FRET in single living cells. *Neuron.* 31:973–985.

Ertel, E. A., K. P. Campbell, M. M. Harpold, F. Hofmann, Y. Mori, E. Perez-Reyes, A. Schwartz, T. P. Snutch, T. Tanabe, L. Birnbaumer, R. W. Tsien, and W. A. Catterall. 2000. Nomenclature of voltage-gated calcium channels. *Neuron.* 25:533–535.

Gao, T., A. J. Chien, and M. M. Hosey. 1999. Complexes of the α_{1C} and β subunits generate the necessary signal for membrane targeting of class C L-type calcium channels. *J. Biol. Chem.* 274:2137–2144.

Haase, H., B. Pfitzmaier, M. W. McEnery, and I. Morano. 2000. Expression of Ca^{2+} channel subunits during cardiac ontogeny in mice and rats: identification of fetal α_{1C} and β subunit isoforms. *J. Cell. Biochem.* 76:695–703.

Helton, T. D., and W. A. Horne. 2002. Alternative splicing of the β_4 subunit has α_1 subunit subtype-specific effects on Ca^{2+} channel gating. *J. Neurosci.* 22:1573–1582.

Hering, S., S. Berjukow, S. Sokolov, R. Marksteiner, R. G. Weiss, R. Kraus, and E. N. Timin. 2000. Molecular determinants of inactivation in voltage-gated Ca^{2+} channels. *J. Physiol.* 528:237–249.

Hoshi, T., W. N. Zagotta, and R. W. Aldrich. 1990. Biophysical and molecular mechanisms of *Shaker* potassium channel inactivation. *Science.* 250:533–538.

Hullin, R., D. Singer-Lahat, M. Freichel, M. Biel, N. Dascal, F. Hofmann, and V. Flockerzi. 1992. Calcium channel β subunit heterogeneity: functional expression of cloned cDNA from heart, aorta and brain. *EMBO J.* 11:885–890.

Iwashima, Y., A. Abiko, F. Ushikubi, A. Hata, K. Kaku, H. Sano, and M. Eto. 2001. Downregulation of the voltage-dependent calcium channel (VDCC) β-subunit mRNAs in pancreatic islets of type 2 diabetic rats. *Biochem. Biophys. Res. Commun.* 280:923–932.

Jeziorski, M. C., R. M. Greenberg, and P. A. Anderson. 2000. Calcium channel β subunits differentially modulate recovery of the channel from inactivation. *FEBS Lett.* 483:125–130.

Jones, L. P., S. K. Wei, and D. T. Yue. 1998. Mechanism of auxiliary subunit modulation of neuronal α_{1E} calcium channels. *J. Gen. Physiol.* 112:125–143.

Kass, R., and M. Sanguinetti. 1984. Inactivation of calcium channel current in the calf cardiac Purkinje fiber. Evidence for voltage- and calcium-mediated mechanisms. *J. Gen. Physiol.* 84:705–726.

Klemic, K. G., C. C. Shieh, G. E. Kirsch, and S. W. Jones. 1998. Inactivation of Kv2.1 potassium channels. *Biophys. J.* 74:1779–1789.

Kukuljan, M., P. Labarca, and R. Latorre. 1995. Molecular determinants of ion conduction and inactivation in K^+ channels. *Am. J. Physiol.* 268: C535–C556.

Ludwig, A., V. Flockerzi, and F. Hofmann. 1997. Regional expression and cellular localization of the α_1 and β subunit of high voltage-activated calcium channels in rat brain. *J. Neurosci.* 17:1339–1349.

Massa, E., K. M. Kelly, D. I. Yule, R. L. MacDonald, and M. D. Uhler. 1995. Comparison of fura-2 imaging and electrophysiological analysis of murine calcium channel α_1 subunits coexpressed with novel β_2 subunit isoforms. *Mol. Pharmacol.* 47:707–716.

Milligan, G., M. Parenti, and A. I. Magee. 1995. The dynamic role of palmitoylation in signal transduction. *Trends Biochem. Sci.* 20:181–187.

Mittman, S., J. Guo, M. C. Emerick, and W. S. Agnew. 1999. Structure and alternative splicing of the gene encoding α_{1I}, a human brain T calcium channel α_1 subunit. *Neurosci. Lett.* 269:121–124.

Olcese, R., N. Qin, T. Schneider, A. Neely, X. Wei, E. Stefani, and L. Birnbaumer. 1994. The amino terminus of a calcium channel β subunit sets rates of channel inactivation independently of the subunit's effect on activation. *Neuron.* 13:1433–1438.

Perez-Reyes, E., A. Castellano, H. S. Kim, P. Bertrand, E. Baggstrom, A. E. Lacerda, X. Y. Wei, and L. Birnbaumer. 1992. Cloning and expression of a cardiac/brain β subunit of the L-type calcium channel. *J. Biol. Chem.* 267:1792–1797.

Peterson, B. Z., C. D. DeMaria, J. P. Adelman, and D. T. Yue. 1999. Calmodulin is the Ca^{2+} sensor for Ca^{2+}-dependent inactivation of L-type calcium channels. *Neuron.* 22:549–558.

Pichler, M., T. N. Cassidy, D. Reimer, H. Haase, R. Kraus, D. Ostler, and J. Striessnig. 1997. β subunit heterogeneity in neuronal L-type Ca2+ channels. *J. Biol. Chem.* 272:13877–13882.

Pitt, G. S., R. D. Zuhlke, A. Hudmon, H. Schulman, H. Reuter, and R. W. Tsien. 2001. Molecular basis of calmodulin tethering and Ca^{2+}-dependent inactivation of L-type Ca^{2+} channels. *J. Biol. Chem.* 276:30794–30802.

Plummer, M. R., and P. Hess. 1991. Reversible uncoupling of inactivation in N-type calcium channels. *Nature.* 351:657–659.

Qin, N., R. Olcese, M. Bransby, T. Lin, and L. Birnbaumer. 1999. Ca^{2+}-induced inhibition of the cardiac Ca^{2+} channel depends on calmodulin. *Proc. Natl. Acad. Sci. USA.* 96:2435–2438.

Qin, N., D. Platano, R. Olcese, J. L. Costantin, E. Stefani, and L. Birnbaumer. 1998. Unique regulatory properties of the type 2a Ca^{2+} channel β subunit caused by palmitoylation. *Proc. Natl. Acad. Sci. USA.* 95:4690–4695.

Qin, N., D. Platano, R. Olcese, E. Stefani, and L. Birnbaumer. 1997. Direct interaction of $G\beta\gamma$ with a C-terminal $G\beta\gamma$-binding domain of the Ca^{2+} channel α_1 subunit is responsible for channel inhibition by G protein-coupled receptors. *Proc. Natl. Acad. Sci. USA.* 94:8866–8871.

Reimer, D., I. G. Huber, M. L. Garcia, H. Haase, and J. Striessnig. 2000. β subunit heterogeneity of L-type Ca^{2+} channels in smooth muscle tissues. *FEBS Lett.* 467:65–69.

Resh, M. D. 1999. Fatty acylation of proteins: new insights into membrane targeting of myristoylated and palmitoylated proteins. *Biochim. Biophys. Acta.* 1451:1–16.

Restituito, S., T. Cens, C. Barrere, S. Geib, S. Galas, M. De Waard, and P. Charnet. 2000. The β_{2a} subunit is a molecular groom for the Ca^{2+} channel inactivation gate. *J. Neurosci.* 20:9046–9052.

Rosenfeld, M. R., E. Wong, J. Dalmau, G. Manley, J. B. Posner, E. Sher, and H. M. Furneaux. 1993. Cloning and characterization of a Lambert-Eaton myasthenic syndrome antigen. *Ann. Neurol.* 33:113–120.

Serrano, J. R., E. Perez-Reyes, and S. W. Jones. 1999. State-dependent inactivation of the α_{1G} T-type calcium channel. *J. Gen. Physiol.* 114: 185–201.

Shi, C., and N. M. Soldatov. 2002. Molecular determinants of voltage-dependent slow inactivation of the Ca^{2+} channel. *J. Biol. Chem.* 277: 6813–6821.

Singer, D., M. Biel, I. Lotan, V. Flockerzi, F. Hofmann, and N. Dascal. 1991. The roles of the subunits in the function of the calcium channel. *Science.* 253:1553–1557.

Sokolov, S., R. G. Weiss, E. N. Timin, and S. Hering. 2000. Modulation of slow inactivation in class A Ca^{2+} channels by β-subunits. *J. Physiol.* 527:445–454.

Stea, A., W. J. Tomlinson, T. W. Soong, E. Bourinet, S. J. Dubel, S. R. Vincent, and T. P. Snutch. 1994. Localization and functional properties of a rat brain α_{1A} calcium channel reflect similarities to neuronal Q- and P-type channels. *Proc. Natl. Acad. Sci. USA.* 91:10576–10580.

Stotz, S. C., J. Hamid, R. L. Spaetgens, S. E. Jarvis, and G. W. Zamponi. 2000. Fast inactivation of voltage-dependent calcium channels. A hinged-lid mechanism? *J. Biol. Chem.* 275:24575–24582.

Stotz, S. C., and G. W. Zamponi. 2001. Structural determinants of fast inactivation of high voltage-activated Ca^{2+} channels. *Trends Neurosci.* 24:176–181.

Tomlinson, W. J., A. Stea, E. Bourinet, P. Charnet, J. Nargeot, and T. P. Snutch. 1993. Functional properties of a neuronal class C L-type calcium channel. *Neuropharmacology.* 32:1117–1126.

Wei, S. K., H. M. Colecraft, C. D. DeMaria, B. Z. Peterson, R. Zhang, T. A. Kohout, T. B. Rogers, and D. T. Yue. 2000. Ca^{2+} channel modulation by recombinant auxiliary β subunits expressed in young adult heart cells. *Circ. Res.* 86:175–184.

Wei, X. Y., E. Perez-Reyes, A. E. Lacerda, G. Schuster, A. M. Brown, and L. Birnbaumer. 1991. Heterologous regulation of the cardiac Ca^{2+} channel α_1 subunit by skeletal muscle β and γ subunits. Implications for the structure of cardiac L-type Ca^{2+} channels. *J. Biol. Chem.* 266: 21943–21947.

West, J. W., D. E. Patton, T. Scheuer, Y. Wang, A. L. Goldin, and W. A. Catterall. 1992. A cluster of hydrophobic amino acid residues required for fast Na^+-channel inactivation. *Proc. Natl. Acad. Sci. USA.* 89: 10910–10914.

Yamada, Y., M. Nagashima, M. Tsutsuura, T. Kobayashi, S. Seki, N. Makita, Y. Horio, and N. Tohse. 2001. Cloning of a functional splice variant of L-type calcium channel β_2 subunit from rat heart. *J. Biol. Chem.* 276:47163–47170.

Yamaguchi, H., M. Okuda, G. Mikala, K. Fukasawa, and G. Varadi. 2000. Cloning of the β_{2a} subunit of the voltage-dependent calcium channel from human heart: cooperative effect of $\alpha_2\delta$ and β_{2a} on the membrane expression of the α_{1C} subunit. *Biochem. Biophys. Res. Commun.* 267: 156–163.

Zagotta, W. N., and R. W. Aldrich. 1990. Voltage-dependent gating of *Shaker* A-type potassium channels in *Drosophila* muscle. *J. Gen. Physiol.* 95:29–60.

Zagotta, W. N., T. Hoshi, and R. W. Aldrich. 1990. Restoration of inactivation in mutants of *Shaker* potassium channels by a peptide derived from ShB. *Science.* 250:568–571.

Zuhlke, R. D., G. S. Pitt, K. Deisseroth, R. W. Tsien, and H. Reuter. 1999. Calmodulin supports both inactivation and facilitation of L-type calcium channels. *Nature.* 399:159–162.

Zuhlke, R. D., and H. Reuter. 1998. Ca^{2+}-sensitive inactivation of L-type Ca^{2+} channels depends on multiple cytoplasmic amino acid sequences of the α_{1C} subunit. *Proc. Natl. Acad. Sci. USA.* 95:3287–3294.